

Influence of topography on coseismic displacements induced by the Friuli 1976 and the Irpinia 1980 earthquakes (Italy) analyzed through a two-dimensional hybrid model

Alberto Armigliato and Stefano Tinti

Department of Physics, Sector of Geophysics, University of Bologna, Bologna, Italy

Received 14 June 2002; revised 13 May 2003; accepted 24 September 2003; published 3 December 2003.

[1] We investigate the perturbations introduced by the local topography on the coseismic displacement components induced by crustal seismic faults. The approach, proposed by *Tinti and Armigliato* [2002], is applicable to homogeneous two-dimensional domains with arbitrary topography of the free surface. It uses both analytical results, valid for homogeneous spaces and half-spaces bounded by a flat free surface (FFS), and a numerical code solving the equations of equilibrium of linear elasticity through a finite element (FE) scheme. A major characteristic of our “hybrid” method is that it allows for the correct representation of the displacement components in correspondence with the fault, which does not need to be explicitly introduced in the FE mesh. We show that, in the case of homogeneous domains, this makes our approach preferable to pure FE schemes. Our hybrid approach is here applied to two different disastrous events of the recent Italian seismic history, for which topography is expected to play an important role, namely the 6 May 1976 ($M_S = 6.5$) Friuli and the 23 November 1980 ($M_S = 6.9$) Irpinia-Basilicata earthquakes. For each event, we selected hypotheses for the parent fault proposed in the literature and compared the coseismic displacements computed through the widely used analytical models dealing with FFS and through our hybrid approach, accounting for the effect of realistic topographies. The most relevant effects are observed in the case of the Irpinia earthquake: depending on the profile chosen, the computed misfits can be as high as 19 and 13% for the horizontal and vertical displacements, respectively, with absolute differences up to 9 and 10 cm.

INDEX

TERMS: 1242 Geodesy and Gravity: Seismic deformations (7205); 7205 Seismology: Continental crust (1242); 7209 Seismology: Earthquake dynamics and mechanics; 7260 Seismology: Theory and modeling;

KEYWORDS: boundary conditions, coseismic displacements, hybrid approach, Friuli 1976 earthquake, Irpinia 1980 earthquake, topography

Citation: Armigliato, A., and S. Tinti, Influence of topography on coseismic displacements induced by the Friuli 1976 and the Irpinia 1980 earthquakes (Italy) analyzed through a two-dimensional hybrid model, *J. Geophys. Res.*, 108(B12), 2552, doi:10.1029/2002JB002027, 2003.

1. Introduction

[2] The modeling of the coseismic displacement field induced by earthquakes in realistic representations of the Earth's crust is one of the classical and more studied problems of modern geophysics. Scientists have been and still are interested in the inclusion of characteristics such as the irregular topography of the Earth's free surface and the crustal heterogeneities in both two- and three-dimensional modeling of the ground deformation under different rheological assumptions. We limit the present introductory overview to the pure elastic approximation of the crust's rheology and to the study of the Earth's surface topography effects. The basic model that is still being widely used in both direct and inverse computations of coseismic displace-

ments is the homogeneous and isotropic elastic half-space bounded by a flat free surface (FFS). A complete set of analytical solutions for the 3-D displacement vector and its derivatives induced by arbitrary point sources and rectangular faults both in the interior and at the surface of the half-space may be found in *Okada's* [1985, 1992] papers. This solution, that we will refer to as “Okada's solution” in the following, is widely used especially in inverse modeling due to its computational convenience. Clearly, it does not allow for modeling the real characteristics of the crust, and in particular for the effect of the irregular topography of the Earth's surface. A trick that is commonly used to overcome this difficulty is to assume a reference elevation corresponding to a sort of “average topography” in the source region, and to add this constant value to the source depth. This approach is not satisfactory for at least two reasons. First, it cannot account for the variability of the topographic relief, that may present large changes even over

very short length scales. Second, the choice of the reference elevation is somewhat arbitrary, depending mainly on the source position and geometry.

[3] More refined methods have been proposed in the literature to model the disturbances introduced by realistic topographies. We can roughly divide them in two main categories. The first includes analytical or semi-analytical approaches, that typically employ series expansion of the FFS half-space solution, yielding a set of higher-order corrections in both 2-D [e.g., *McTigue and Mei*, 1981; *McTigue and Stein*, 1984; *Meertens and Wahr*, 1986; *McTigue and Segall*, 1988; *Volynets and Voevoda*, 1992] and 3-D [*Voevoda and Volynets*, 1992; *Williams and Wadge*, 2000]. The limitation of these methods is that they are based on the expansion of the reference FFS half-space solution in powers of a characteristic parameter ε that must be small ($\varepsilon \ll 1$). Possible definitions for the “small parameter” are $\varepsilon = H/L$, where H and L are the characteristic vertical and horizontal scales of the topography [*McTigue and Mei*, 1981; *McTigue and Segall*, 1988; *Williams and Wadge*, 2000], or $\varepsilon = H_{max}/d$, H_{max} and d being respectively the maximum value of the topography and the depth of the fault top [*Volynets and Voevoda*, 1992; *Voevoda and Volynets*, 1992]. As a consequence, only small-slope and/or small-magnitude topographies can be treated by these methods.

[4] The second category is composed by the large family of numerical methods, such as finite elements (FE), boundary elements, and finite differences. Here we will limit our attention to the approaches based on the FE technique, since it proves to be probably the most suitable to deal with irregular boundaries, and hence the best choice if we are interested in the realistic representation of the Earth crust’s irregular topography. Both 2-D and 3-D FE models can be found in the literature: it will be sufficient to recall here the paper by *Harrison* [1976], where the attention was focused on the disturbances introduced by topography on surface tilt and strain measurements, and the more recent study by *Huang and Yeh* [1997], who performed a set of theoretical experiments on the effects of synthetic topographies on surface displacements for different fault geometries, mechanisms and positions with respect to the relevant topographic features. Notwithstanding the possibility to treat accurately even very complicated geometries, the pure FE schemes present an important drawback related to the representation of the coseismic displacement field in correspondence with the fault plane. Typically, the fault must be introduced directly in the FE mesh as an internal boundary, and this is accomplished through various possible techniques: for example, the fault plane can be defined by a series of pairs of adjacent nodes, or more conveniently by a single line of so-called “split nodes” [*Melosh and Raefsky*, 1981]. In any case, appropriate boundary conditions, e.g., displacements, have to be prescribed on the fault nodes, meaning that the selected conditions must be known a priori. For instance, if we take into consideration the case of a shear fault with a slip vector of magnitude Δu , we can choose to assign exclusively the discontinuous tangential displacement on the fault nodes: if the fault is represented by a set of adjacent nodes, the absolute tangential displacement on each side of the fault must be prescribed (e.g., $\pm\Delta u/2$), while in the case of the split-node technique it suffices to assign the relative displacement Δu .

[5] Whichever the selected technique is, the need for the assignment of boundary conditions that must be known a priori on the fault nodes may lead to partially incorrect results, as turns out from the results of the studies by *Bonafede and Neri* [2000] and by *Armigliato et al.* [2003a, 2003b]. They pointed out that, in the coseismic limit, the fault plane undergoes a quite complicated deformation even in the simplest case of a half-space with FFS. In particular, the fault plane experiences displacements along both the tangential and the normal directions. Two main contributions to these displacements can be recognized. The first is related to the source itself, and in particular to the double-couple equivalent representation of the dislocation process: we will call it “Source Term” and denote it as ST according to *Armigliato et al.* [2003a, 2003b], whose main results are here summarized. In the case of a shear fault, ST is responsible for a discontinuous and anti-symmetric tangential component, being equal to the imposed differential slip, and for a continuous and non-uniform normal component. The second contribution is a correction introduced by the presence of the free surface, and will be denoted as FSC (standing for “Free Surface Correction”). The FSC regards both the normal and the tangential components, except for the case of vertical faults in a homogeneous half-space, for which the tangential FSC vanishes. Both normal and tangential FSC are continuous and not uniform across the fault plane. Moreover, the tangential FSC orientation is consistent with the ST tangential displacement on the fault upper surface and its modulus can be as high as 20% of the imposed shear slip for shallow sources with the consequence that the intrinsic anti-symmetry in the tangential ST is lost in the final solution. What is important to point out here is that FSC depends on the shape of the free surface and that it is possible to compute it exactly only in the basic case of homogeneous FFS half-spaces. Pure FE models, which require the “a priori” knowledge of the displacements (absolute or relative) to be assigned on the fault nodes, can fail partially, or even totally, to account for FSC and we will show in the next section that this shortcoming may lead to incorrect results for the surface coseismic displacements.

[6] In the present study, the modeling of the effect of the irregular topography of the Earth’s free surface is faced by applying a two-step approach recently proposed by *Tinti and Armigliato* [2002, hereinafter referred to as T&A]. It is valid for 2-D homogeneous, isotropic, elastic domains delimited by irregular free surface boundaries and it uses both the analytical results valid for homogeneous spaces and FFS half-spaces, and a numerical code we developed which solves the equations of equilibrium of linear elasticity through a finite element scheme in the plane-strain approximation. A relevant characteristic of our “hybrid” method, and at the same time a key difference with respect to pure FE codes, is that we don’t need to introduce the fault into the FE mesh explicitly, which brings two main advantages. The first is that we are able to compute a solution accounting for the complete displacement field in correspondence with the fault plane, the second is that we don’t need to build a new FE mesh each time we change the fault geometry and/or position. In the next section we will describe the main characteristics of the approach and discuss a couple of basic examples where the results

obtained through our method are compared to those computed via a pure FE technique.

[7] Afterward, we will discuss the application of the method to two events of the recent Italian seismic history, occurred in regions exhibiting interesting topographic features. The first case study is the May 6, 1976 earthquake ($M_S = 6.5$) that hit the Friuli region in north-eastern Italy, whose epicenter has been located in the eastern alpine relief. The second is represented by the November 23, 1980 shock ($M_S = 6.9$) occurred in the Irpinia-Basilicata region, which is found in correspondence with a portion of the southern Apennine chain. Our approach consists in selecting one of the fault models proposed in the available literature for each of the two events and in comparing the surface coseismic displacements obtained by means both of the analytical formulae valid for FFS and of our hybrid technique accounting for topography effects.

2. The Model

2.1. General Description

[8] The main features of the model introduced by T&A are here recalled by the aid of Figure 1. We adopt a perfectly elastic, homogeneous and isotropic finite 2-D domain A as an approximate representation of a limited vertical cross-section of the Earth's crust. The external boundary of A , that we will indicate with Γ , is partitioned into two portions Γ_1 and Γ_2 , such that $\Gamma = \Gamma_1 \cup \Gamma_2$. The portion Γ_1 represents the free surface of the Earth's crust and can assume any arbitrary shape, while Γ_2 coincides with the buried part of the boundary, that we will refer to as the "crustal boundary". Note that, in principle, Γ_2 can assume any form, but, for the kind of applications we are interested in, the simplest choice will be to represent Γ_2 as a portion of a rectangular boundary. A fault F with dip angle δ and constant dislocation vector $\mathbf{d}(F)$ is entirely comprised within A . The domain is discretized by means of a FE mesh consisting of triangular elements, particularly suitable to represent irregular boundaries. Our goal is to find the solution to the equations of elastic equilibrium:

$$\sigma_{ij,j} = 0 \quad i,j = 1, 2 \quad (1)$$

in terms of the displacement vector $\mathbf{u}(A)$ in each of the nodes of the FE grid. To do this, we express the total solution $\mathbf{u}(A)$ as the sum of two distinct terms, to be computed in two separate steps:

$$\mathbf{u}(A) = \mathbf{u}_{\text{ST}}(A) + \mathbf{u}_{\text{FSC}}(A) \quad (2)$$

[9] The first term $\mathbf{u}_{\text{ST}}(A)$ is related to the seismic source itself and univocally defined by $\mathbf{d}(F)$. It is the displacement field that would be induced by the dislocation if it was embedded in an infinite homogeneous elastic space, and it can be computed through the analytical formulae valid for homogeneous spaces (see Okada, 1992). In particular, ST induces the tractions $\mathbf{t}_{\text{ST}}(\Gamma_1)$ and the displacements $\mathbf{u}_{\text{ST}}(\Gamma_2)$. Further, we define an ancillary solution $\mathbf{u}_{\text{OK}}(\Gamma_2)$ for the displacement that is computed as follows. The domain A is replaced with the domain A_{OK} having the same crustal boundary as A but a flat free surface Δ_1 connecting the same ends as Γ_1 . Observe that A_{OK} may be viewed as a

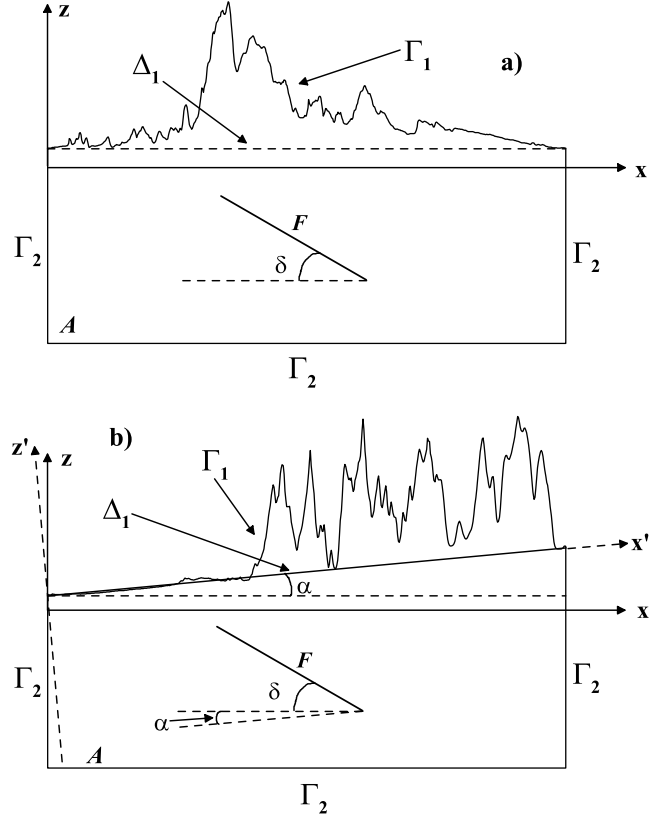


Figure 1. Sketch of the model adopted in this paper. Γ_1 and Γ_2 are the free surface boundary and the crustal boundary of the elastic domain A , respectively. In general, Γ_1 is characterized by an irregular shape representing the Earth's surface topography. Δ_1 is the FFS boundary connecting the same ends as Γ_1 , and it is introduced to compute Okada's solution on the crustal boundary Γ_2 . In a) Δ_1 is parallel to the x axis, while in b) it forms a non negligible angle α with the x direction. See text for further details.

limited portion of a half-space in which a fault F with given dislocation $\mathbf{d}(F)$ is embedded. The idea is then to compute the solution $\mathbf{u}_{\text{OK}}(\Gamma_2)$ through the analytical formulae by Okada [1992], which are valid when the two ends of the surface boundary have the same $z = 0$ elevation. In general this is not true for realistic topographic profiles. In the present discussion we examine two different cases, portrayed in Figures 1a and 1b respectively. In the first (Figure 1a), the two extremes of Δ_1 have the same z value, so that the Okada condition can be fulfilled by a simple translation along the z axis. In the second case (Figure 1b), Δ_1 forms a small but not negligible angle α with the direction of the x axis: we can apply Okada's formulae only if we express all the relevant model parameters and perform the computations in the roto-translated reference system defined by the axes x' and z' . Once the solution has been obtained in the rotated reference system, we can revert it back in the original reference system to obtain the required boundary solution $\mathbf{u}_{\text{OK}}(\Gamma_2)$. It is worth mentioning that this second case represents an enhancement of the original procedure by T&A.

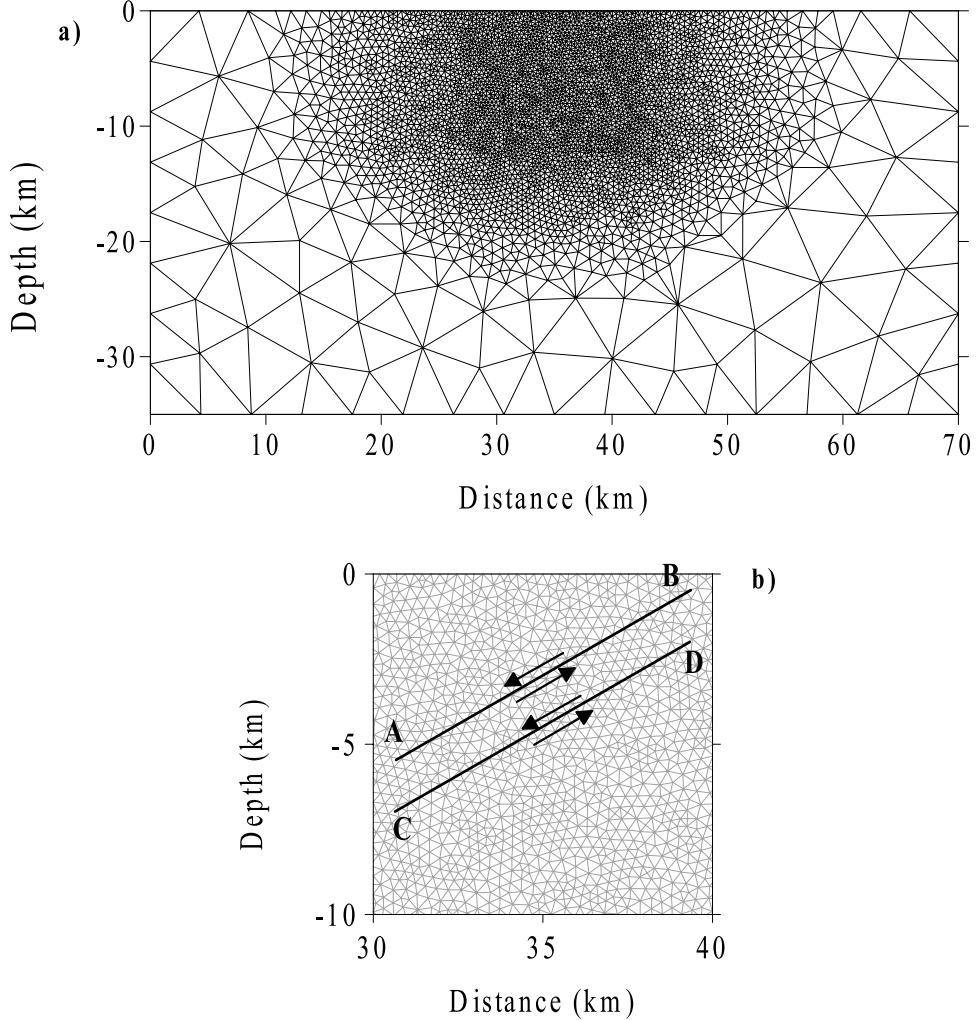


Figure 2. (a) The FFS elastic domain used to perform the theoretical experiments described in section 2.2, and the FE mesh built to discretize it, formed by 4487 nodes and 8806 triangular elements. (b) Close-up view of the two faults adopted in the tests. They share the same width $W = 10$ km, dip angle $\delta = 30^\circ$, normal mechanism and uniform slip $U = 1$ m: moreover, their centers of mass have the same abscissa $x = 35$ km. They differ with respect to the upper edge depth d , which is $d = 500$ m for fault AB and $d = 2$ km for fault CD.

[10] The second term in (2), $\mathbf{u}_{\text{FSC}}(A)$, is the correction that must be added to ST when a free surface is introduced in the model. This term can be computed exactly only in the very particular case of a flat free surface. Since we are interested in irregular topographies, we compute $\mathbf{u}_{\text{FSC}}(A)$ numerically by solving a linear elasticity problem in the plane-strain approximation via a FE code we developed, with boundary conditions imposed as follows:

$$\mathbf{t}_{\text{FSC}}(\Gamma_1) = -\mathbf{t}_{\text{ST}}(\Gamma_1) \quad (3a)$$

$$\mathbf{u}_{\text{FSC}}(\Gamma_2) = \mathbf{u}_{\text{OK}}(\Gamma_2) - \mathbf{u}(\Gamma_2) \quad (3b)$$

In conclusion, the final solution given by definition (2) is characterized by null traction on the free surface boundary Γ_1 and by displacements equal to Okada's, i.e., computed in the case of a flat free surface, in all the nodes belonging to the crustal boundary Γ_2 . In other words, we assume that the

conditions “at infinity” are exactly the same in presence both of an irregular free surface boundary Γ_1 and of a flat boundary Δ_1 .

2.2. Comparison With Pure Finite Element (FE) Codes on the Flat Free Surface (FFS) Reference Case

[11] The validity of the two-step technique described above has already been thoroughly discussed by T&A, who checked the numerical results against the analytical Okada's solution in the case of faults with different dip angles and mechanisms, buried in a FFS half-space. Taking the same basic model, i.e., a homogeneous half-space with FFS, as a reference case, we are here interested in comparing the surface coseismic displacements obtained through our method and through a pure FE technique with two different choices for the boundary conditions in correspondence of the fault nodes. With reference to Figure 1, the selected domain A is a portion of a Poissonian homogeneous half-space characterized by a rigidity $\mu = 3 \cdot 10^{10}$ Pa.

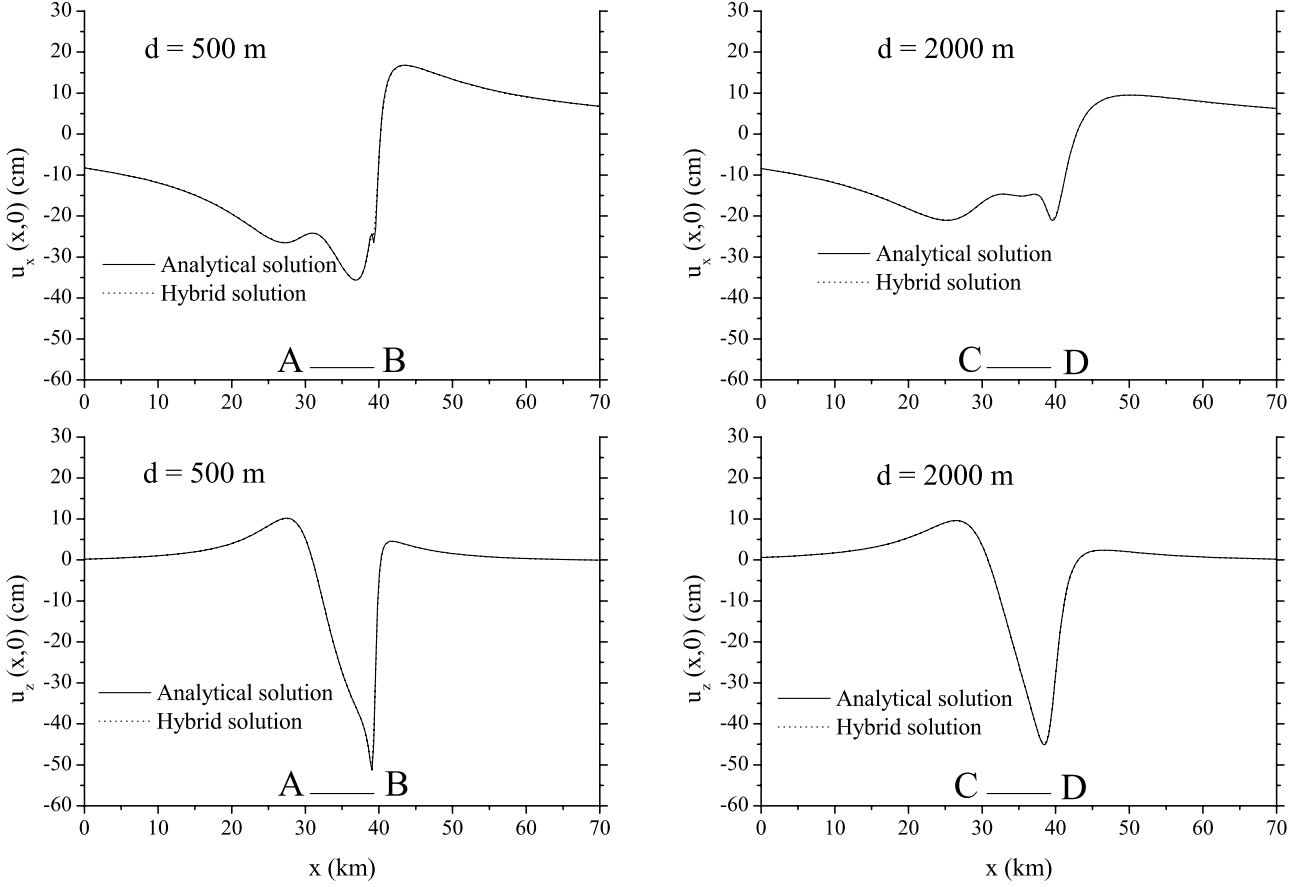


Figure 3. Comparison between the results obtained through Okada's analytical formulae (solid lines) and through our two-step hybrid approach. The panels on the left refer to the horizontal and vertical displacements for the shallower fault, while those on the right are related to the deeper fault. Note that in all panels the two solutions are very close and almost undistinguishable.

The domain is portrayed in Figure 2a: its dimensions are 70 km along the x coordinate and 35 km along the z direction, and it has been discretized with a FE mesh composed of 4487 nodes and 8806 elements. For the tests presented here we chose the class of faults having width $W = 10$ km, dip angle $\delta = 30^\circ$ and a pure normal mechanism with uniform slip $U = 1$ m. Since we adopt a 2-D plane-strain approximation, the fault length L should be theoretically much larger than the typical size of the selected (x, z) domain: we found that a good approximation is to take $L = 20W$. Two faults were chosen, with depth d of the upper edge equal to $d = 500$ m and $d = 2000$ m (segments AB and CD in Figure 2b). For both faults, the center of mass lies on the vertical symmetry axis at $x = 35$ km. The mesh depicted in Figure 2a, as well as all the other FE meshes we will present throughout this paper, were built by assigning the finest resolution to the region in which the fault lies, that is to say in the portion of the domain in which the highest gradients for the displacement and traction fields are expected. Figure 3 shows the matching between the surface displacement curves obtained through Okada's formulae (solid lines) and our hybrid technique (dotted lines). In particular, the leftmost panels displays the horizontal and vertical signals computed for the shallower fault ($d = 500$ m, segment AB in Figure 2b), while in the rightmost panels the

results for the deeper fault ($d = 2000$ m, segment CD in Figure 2b) are reported. The quality of the matching can be quantified by computing separate misfits μ_x and μ_z for the displacement components u_x and u_z according to the following formulae:

$$\mu_x = \sqrt{\frac{\sum_{i=1}^N (u_x^{ref} - u_x^c)^2}{\sum_{i=1}^N (u_x^{ref})^2}}; \quad \mu_z = \sqrt{\frac{\sum_{i=1}^N (u_z^{ref} - u_z^c)^2}{\sum_{i=1}^N (u_z^{ref})^2}} \quad (4)$$

where N is the number of points describing the Γ_1 boundary in the FE mesh. For the case studied in Figure 3, u_x^{ref} and u_z^{ref} are the analytical Okada's displacements along the x and z axes, respectively, while u_x^c and u_z^c are the corresponding displacements computed through our hybrid approach. Table 1a contains the results relative to Figure 3: the matching is in general satisfactory, with minor discrepancies

Table 1a. Misfits Between the Solutions Illustrated in Figure 3

	μ_x , %	μ_z , %
$d = 500$ m	1.8	2.4
$d = 2000$ m	0.8	0.6

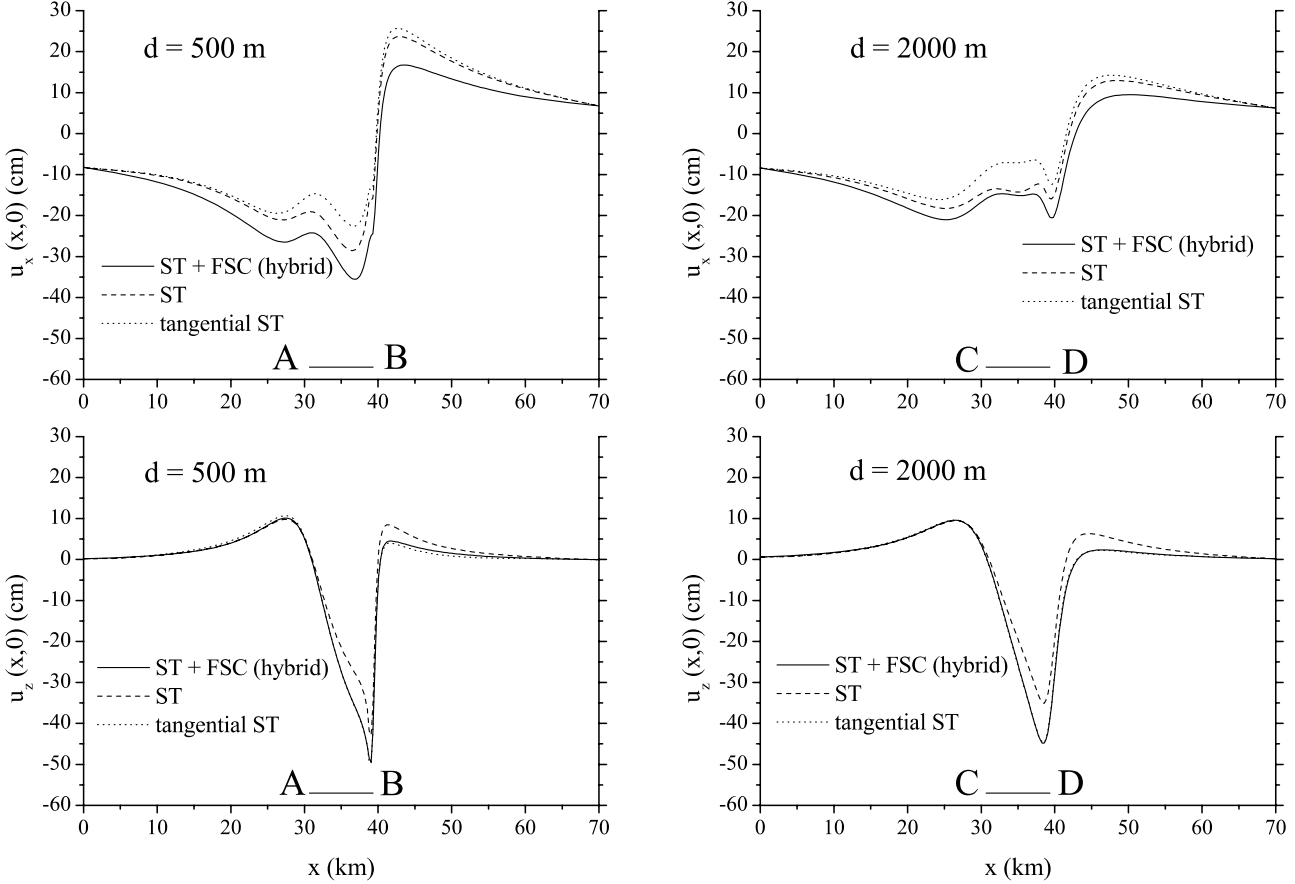


Figure 4. Comparison between the displacements computed by means of our approach and of a pure FE technique in which two different choices for the displacements to be assigned on the fault boundary have been adopted. The solid curve (ST+FSC) has been obtained with our model, accounting for both the source term and the free surface correction term (ST+FSC). The other two curves are the output of a pure FE code where the displacements assigned on the fault coincide with the complete source term (ST) and with the single anti-symmetric tangential source displacement (tangential ST).

appreciable only in correspondence with the surface projection of the fault upper edge. Note further that the matching improves as the fault becomes deeper.

[12] Let us now discuss the comparison between the signals computed, for the same two faults, a) through our hybrid technique and b) by means of a pure FE approach, that implies inserting the fault explicitly in the FE mesh and imposing given displacements on the fault nodes. The results are summarized in Figure 4, where, as in Figure 3, the leftmost and rightmost panels are relative to the shallower and the deeper faults, respectively. Three curves are plotted in each panel. The solid lines, labeled as “ST+FSC”, are obtained through our method and will be taken as “reference curves”. The label “ST+FSC” indicate that the hybrid technique is able to account both for the source term and for the free surface correction on the fault plane, and is then expected to provide the “correct” representation of the physics of the problem. The other two curves are obtained through a pure FE approach, i.e., through a pure numerical approach in which the fault is introduced in the FE mesh and represented as a series of adjacent pairs of nodes, and refer to two different possible choices of the displacements imposed on the fault nodes. The label “ST” indicate that the complete displacement

field related to the source term has been imposed on the fault boundary, that is to say that we assigned both the tangential and normal displacement components computed through the subset of the Okada’s analytical formulae valid for a fault buried in an infinite homogeneous elastic space. The second choice, denoted by the “tangential ST” label, consists in assigning the sole anti-symmetric tangential displacement, leaving the normal displacements as unknowns of the problem. In general, other choices for the fault boundary conditions are possible: here we just selected two options that seem reasonable when it is not possible to compute FSC “a priori”. The results in Figure 4 clearly indicate that, even in the simple case of a FFS, none of the results obtained through the pure FE approach is able to completely reproduce the reference curves. Very similar observations hold for both the shallower and the deeper fault cases. Concerning the results relative to the first choice (“ST”), discrepancies can be observed in both the horizontal and the vertical displacements: in the case of the horizontal component the discrepancy regards the entire signal, while it affects mainly the region around the fault projection for the vertical one. The “tangential ST” choice leads to a very good fit in the vertical signals, but to a misfit in the horizontal component that is even larger than that

Table 1b. Misfits and Maximum Absolute Differences Between the Solutions Illustrated in Figure 4

	μ_x , %	μ_z , %	$ \Delta u_x _{\max}$, cm	$ \Delta u_z _{\max}$, cm
(ST+FSC)-ST($d = 500$ m)	25	22	10.9	9.1
(ST+FSC)-ST($d = 2000$ m)	19	28	5.4	9.9
(ST+FSC)-tangential ST($d = 500$ m)	35	4.1	13.6	2.7
(ST+FSC)-tangential ST($d = 2000$ m)	36	1.7	8.5	0.9

relative to the “ST” choice. Quantitative values for the misfits computed through formulae (4) are given in Table 1b: note that, in this case, u_x^{ref} and u_z^{ref} are the displacements components computed through our hybrid method (“ST+FSC”), while u_x^c and u_z^c represent one after the other the “ST” and the “tangential ST” results. In addition to μ_x and μ_z , we also provide the maximum absolute differences between the hybrid and the pure FE signals for both displacement components ($|\Delta u_x|_{\max}$ and $|\Delta u_z|_{\max}$).

[13] These simple examples unequivocally show that neglecting the FSC terms can lead to distorted results for the surface coseismic displacements. The discrepancies are expected to increase for shallower faults.

3. The Friuli 1976 Earthquake

[14] The Friuli region, located in the northeastern part of Italy, is interested by complex tectonic processes, that are mainly related to the active collision between the Eurasian and Adriatic plates [Anderson and Jackson, 1987; Bressan *et al.*, 1998; Slepko *et al.*, 1999]. The compressional tectonic regime is responsible for the orogenic processes that led to the formation of the two main structural units present in the region, that is to say the Southern Alps and the Dinaric chain, which merge together in central Friuli. Different faults have been recognized in this area, consisting mainly in E-W and SE-NW striking overthrusts dipping northward with shallow angles. To the west, this fault system is intersected by a system of sub-vertical faults striking N-S and mainly characterized by strike-slip motion. Earthquake catalogues [e.g., Boschi *et al.*, 1997] indicate that several destructive events occurred in the region, among which it is worth citing the January 25, 1348 and the March 26, 1511 shocks with estimated magnitudes 6.6. and 6.8, respectively.

[15] The last destructive earthquake sequence hitting the Friuli region occurred between May and September 1976. On May 6, 1976, 20:00 GMT a $M_S = 6.5$ earthquake struck the area, reaching a maximum intensity of X (MCS) and producing many casualties and severe damage in several localities. The main shock was preceded by a $M_S = 4.5$ foreshock and followed by a long aftershock sequence till September 1977, culminating in two strong events on September 15, 1976 at 03:15 GMT ($M_S = 6.0$) and at 09:21 GMT ($M_S = 6.1$). A sketch of the region and of its topographic relief (extracted from a recent Italian DTM provided by the Politecnico of Milano, Italy) is plotted in Figure 5. The epicenters of the three most energetic events of the sequence, i.e., the May 6 main shock and the two aftershocks occurred on September 15 are indicated by the solid star, diamond and square, respectively. In correspondence with each event we plotted the respective fault plane solution proposed by Aoudia *et al.* [2000].

[16] Here we will limit our attention to the main shock of May 6, 1976. An abundant literature is available concerning the determination of the main characteristics of the genetic fault on the basis of the analysis of different data-sets. For example, Briole *et al.* [1986] performed detailed modeling of the leveling data described by Talamo *et al.* [1978]. More recent studies were focused on the inversion of ground acceleration data [Zollo *et al.*, 1997] or on analyses combining hypocenters relocation, long period surface wave

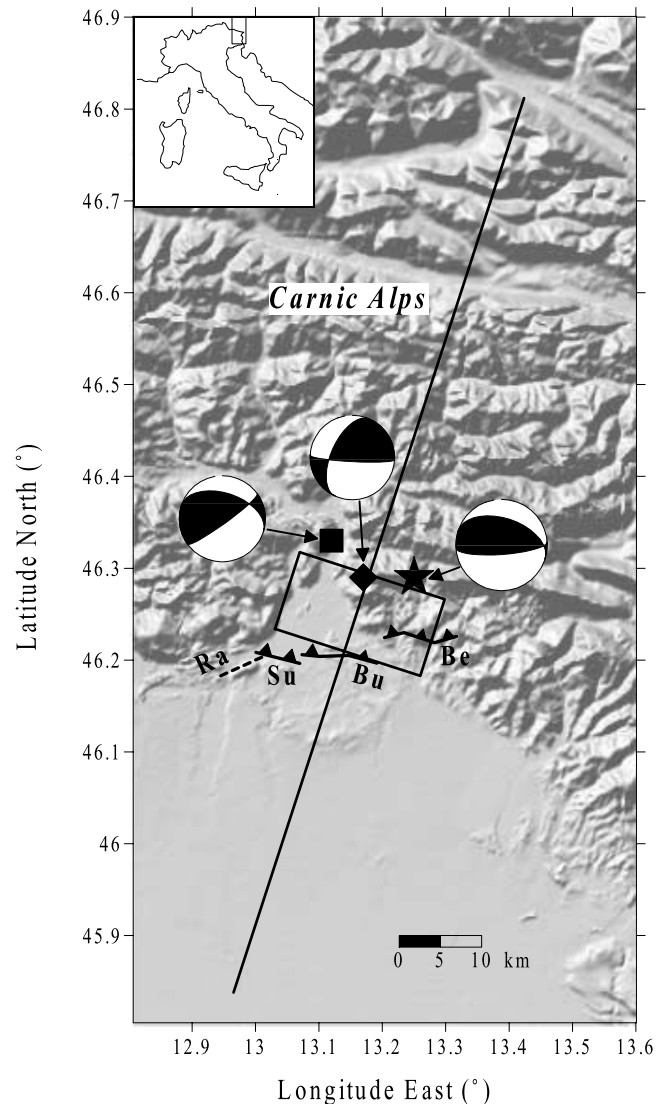


Figure 5. Topographic map of the region hit by the 1976 earthquake sequence. Fault plane solutions and epicenter locations from Aoudia *et al.* [2000]: the three solid symbols indicate respectively the epicenters of the May 6 main shock (star) and of the September 15 aftershocks (diamond – 3:15 GMT, square – 9:21 GMT). The Bernadia (Be), Buia (Bu) and Susans (Su) ridges and the Ragona (Ra) fold have been proposed as possible surface expressions of the rupture process. The surface projection of the north-dipping reverse fault proposed by Aoudia *et al.* [2000] for the May 6 main shock is represented as a black bordered rectangle, while the long black line is the intersection with the free surface of the 2-D cross-section chosen for our computations.

Table 2. Fault Parameters for the Earthquakes Occurring in Friuli on 6 May 1976 (derived from *Aoudia et al.* [2000]) and in Irpinia-Basilicata on 23 November 1980 (from *De Natale et al.* [1988] and *Pingue et al.* [1993])

Fault Parameters	Friuli, 6 May 1976	Irpinia-Basilicata, 23 November 1980
strike	288°	317°
dip	29°	71°
rake	112°	270°
M_0 (10^{19} Nm)	0.57	1.5
L, km	18.5	23.345
W, km	11.2	8.6
ΔU , m	0.92 (heterogeneous)	2.5
Top depth (d), km	1.5	3.2

inversion and strong motion modeling [*Aoudia et al.*, 2000]; it is also worth recalling the work by *Pondrelli et al.* [2001], who relocated the earthquakes of the sequence and computed centroid-moment tensors, taking also into account geodetic measurements and geological evidences. It is not the goal of the present study to discuss the different hypotheses nor to propose a model for the parent fault, which is still an open problem: we are rather interested in selecting a fault hypothesis among those proposed so far and in performing a direct modeling of the effect of topography on the expected coseismic displacements.

[17] The adopted model is the one proposed by *Aoudia et al.* [2000]. The seismogenic structure is defined in terms of a fault-related folding with varying characteristics along the strike direction: it starts as a blind fault beneath the Bernadia

and Buia ridges (indicated with codes “Be” and “Bu” in Figure 5), then it changes into a semi-blind structure beneath the Susans ridge and ends up in correspondence of the Ragogna fold (respectively “Su” and “Ra” in Figure 5). The surface projection of the proposed fault is represented as a black-bordered rectangle in Figure 5, while its main parameters are summarized in Table 2. Note that only a small portion of the fault projection is placed in correspondence with relevant topographic features. Some remarks are due at this point concerning the representation of this fault in our 2-D model. First, since we work under a plane-strain approximation, the fault length is assumed as theoretically infinite: as we discussed in sub-section 2.2, a reasonable approximation is to choose a fault length $L = 20W$. Second, the rake angle of 112° indicates that the focal mechanism consists mainly in a thrust with a minor strike-slip component: since our computations are limited to two dimensions, we assume a pure thrust mechanism. Last, the slip distribution modeled by *Aoudia et al.* [2000] is significantly heterogeneous, with three main patches of energy release placed in correspondence of the Bernadia, Buia and Susans faults: we are not able to reproduce slip variations along the strike direction, hence we will simply take into consideration a fault with constant slip. Note that none of the cited approximations are decisive in the context of the present approach, where the interest is focused on the effect of the local topography on surface coseismic displacements rather than on those related to the details of the rupture process.

[18] Referring again to Figure 5, the chosen 2-D cross-section intersects the free surface along the black line that

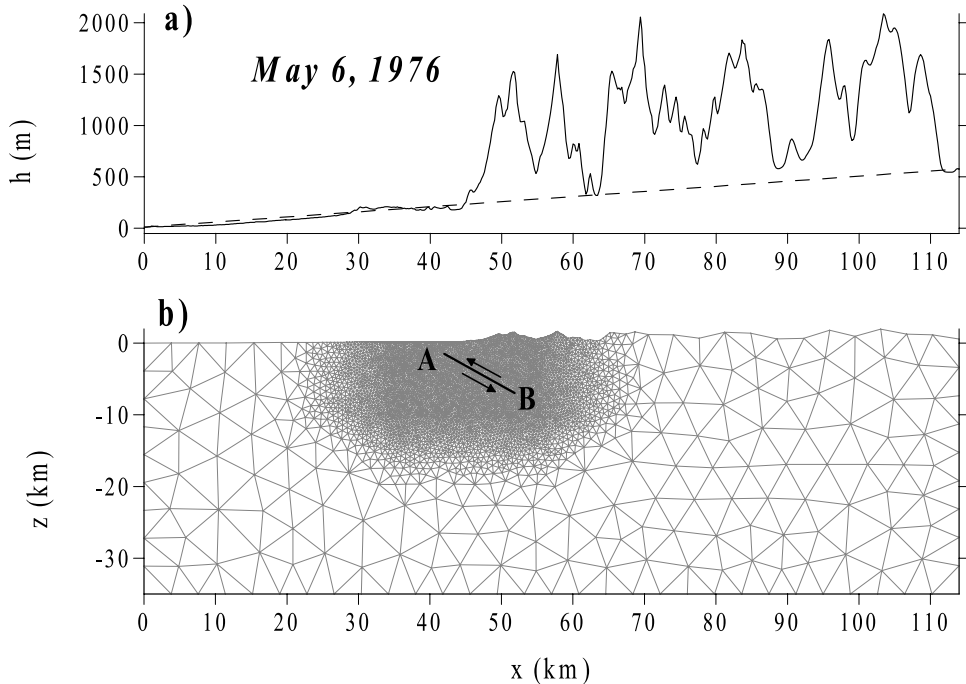


Figure 6. (a) Topographic relief along the surface profile of the 2-D cross-section (black line in Figure 5). The dashed line represents the FFS boundary Δ_1 used to compute the ancillary Okada's solution on the crustal boundary Γ_2 (see Figure 1b). The vertical scale is highly exaggerated. (b) Global view of the cross-section and of the relative FE mesh: it is formed by 5465 nodes and 10,701 triangular elements. The segment AB represents the *Aoudia et al.* [2000] fault plane: the resolution of the FE mesh near the fault is in the order of 250 m, comparable with that of the DTM employed.

cuts the fault projection approximately in its central part. The topographic profile along the cross-section is depicted in Figure 6a, while Figure 6b shows the FE mesh used to discretize the domain. The highest resolution is assigned to the neighborhood of the fault, represented by the black segment AB in Figure 6b. The typical triangles size in this subdomain is in the order of 250 m. Our goal is to compare the surface displacement components induced by the selected fault model along the chosen profile, computed 1) through our hybrid technique, accounting for the topography effect, and 2) through Okada's analytical formulae, valid for FFS. When computing the latter solutions, we must choose some sort of "equivalent flat reference level", that will be indicated as h_e : if d denotes the depth of the top of the fault with respect to the $z = 0$ plane, $h_e + d$ will indicate the depth of the top of the equivalent Okada's fault. The three different choices adopted here for h_e are displayed in the central panel of Figure 7, together with the topography along the profile. With reference to the discussion developed in sub-section 2.1 and in particular to Figure 1b, it is worth observing that the extremes of the topographic

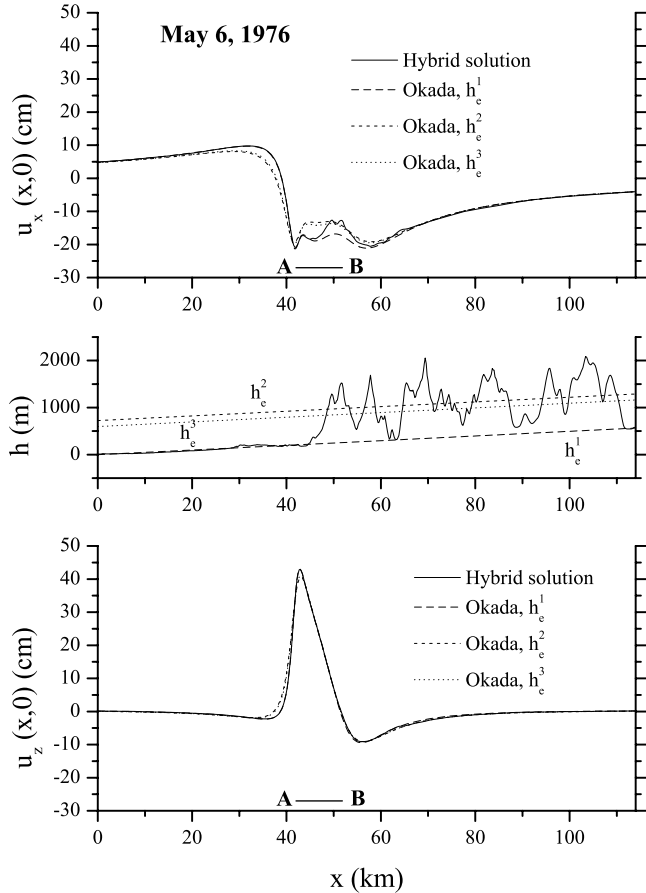


Figure 7. Horizontal (upper panel) and vertical (lower panel) surface coseismic displacements for the May 6, 1976 Friuli earthquake. Segment AB indicates the surface projection of the fault shown in Figure 6. The central panel contains the topographic relief and the three equivalent flat surface boundaries: $h_e^1 = 0$, $h_e^2 = 724$ m (topography averaged on the entire profile), $h_e^3 = 598$ m (topography averaged on the sub-interval $x \in [35, 58]$ km).

Table 3. Misfits and Maximum Absolute Differences Between the Solutions Accounting for Topography and Those Computed Through Okada's FFS Model for the Two Earthquakes Studied in This Paper

	μ_x , %	μ_z , %	$ \Delta u_x _{\max}$, cm	$ \Delta u_z _{\max}$, cm
Friuli	13	2	4.6	1.0
Irpinia profile 1	16	13	9.3	10.4
Irpinia profile 2	19	9	6.9	8.5

profile have markedly different elevations: in this case h_e must be referred to a roto-translated reference system, the rotation angle being defined by the direction of the x axis and the line connecting the two ends of the profile. The three choices for h_e correspond respectively to the "zero elevation" level in the rotated reference system (h_e^1), to the topography average value computed on the entire profile (h_e^2) and on the sub-interval $x \in [35, 58]$ km containing the source surface projection (h_e^3).

[19] The top and bottom panels of Figure 7 illustrate the comparative results for the horizontal and vertical displacement components, respectively: in both panels the same scale has been adopted for the vertical axes. As regards the vertical displacement, the curves computed through our hybrid approach and by means of Okada's formulae for h_e^1 are almost superimposed. Minor differences are observable in the comparison with the curves computed for h_e^2 and h_e^3 : in particular, the two signals are slightly reduced with respect to the one accounting for topography in correspondence with the surface projection of the fault upper edge (A) and slightly amplified in the points belonging to a small interval to the left of the fault. More significant differences can be appreciated on the horizontal signals (top panel in Figure 7), especially near the source surface projection. The analytical solution computed for h_e^1 fits rather well the solution accounting for topography in the far field and also in a small interval around the fault upper edge projection A: as we move toward the projection of the lower edge of the fault B, the two curves become clearly distinguishable, with the analytical signal being amplified with respect to the numerical one. The behavior of the other two analytical curves computed for h_e^2 and h_e^3 is in a certain sense opposite: the fit with the curve including the topography correction is rather satisfying in the points close to the fault lower edge surface projection, while it is worse in correspondence with the upper part of the fault and with an interval about 10 km long to the left of the fault. Moreover, the local topography induces high frequency irregularities on the horizontal displacement which are not observed in the analytical signals. The qualitative remarks are confirmed by the values for the misfits and for the maximum absolute differences listed in Table 3. The comparison is made between the curve accounting for topography, taken as reference, and the FFS solution obtained for h_e^1 : moreover, the computations are limited to the points lying in the sub-interval $x \in [36.5, 57.5]$ km obtained adding half of the fault width at both ends of its surface projection AB. The misfit on the horizontal displacement (13%) is much more relevant than the misfit found for the vertical component (2%); the same holds for the maximum absolute differences, which are found in a node placed close to the surface projection of

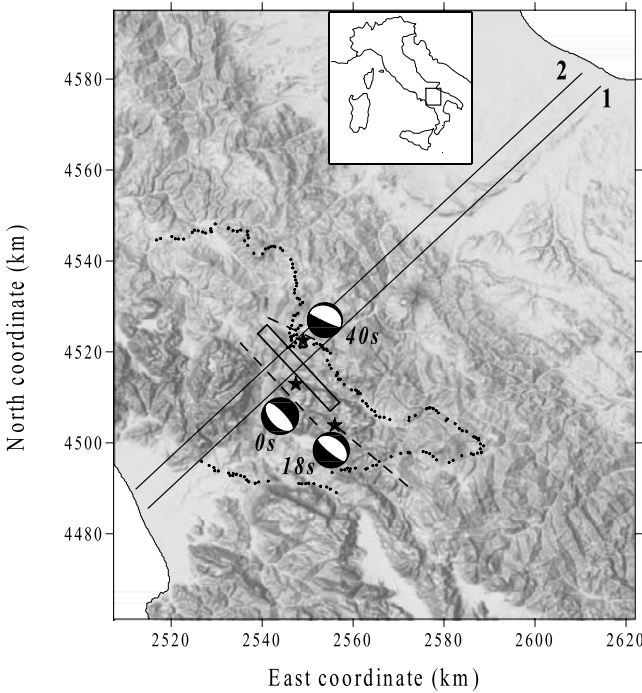


Figure 8. Geographic location and topographic map of the Irpinia-Basilicata region hit by the November 23, 1980 earthquake. East and North coordinates are expressed in the Gauss-Boaga reference system. The small black circles indicate the leveling benchmarks where vertical elevation changes before and after the event were measured. Black stars are the epicenters of the three main subevents associated with the main shock (from *Bernard and Zollo* [1989]): the dashed segments indicate the upper edge surface projection of the three-subfault model by *Pingue et al.* [1993], whose mechanisms are described by the focal spheres. The black-bordered rectangle is the single-fault model adopted in this study, elaborated by *De Natale et al.* [1988] and *Pingue et al.* [1993], while the long solid lines represent the two profiles along which we performed our simulations.

the deeper end of the fault. The pronounced difference between the effects on the horizontal and vertical signals may be partly imputed to very shallow dip angle of the fault. Note further that the difference $|\Delta u_z|_{\max}$ amounts only to 1 cm, which is comparable to the characteristic error of the leveling data available for the Friuli earthquake: we can then conclude that, for this particular earthquake, the Okada FFS model is sufficient to model the observed deformation field. The main reason for the small influence of topography on the vertical deformation should be found in the position of the fault relative to the topography itself: as we already observed with regard to Figure 5, the surface projection of the fault proposed by *Aoudia et al.* [2000] intersects the topographic relief only marginally, specifically in correspondence with the deeper portion of the fault.

4. The Irpinia 1980 Earthquake

[20] On November 23, 1980, 18:34 GMT, an earthquake of magnitude $M_S = 6.9$ severely struck a very large area of the southern Apennines. The Irpinia and Basilicata regions

experienced the most devastating effects: in particular, in Irpinia, corresponding with the epicentral area, degree X of the MCS intensity scale was reached. Several villages were almost completely destroyed and about 3000 people were killed. Figure 8 shows a geographical sketch of the interested regions and a shaded relief map of the topography. This earthquake has been, and still is, of great interest for the scientific community not only for the very large amount of collected data, which makes of it one of the best documented Italian seismic events, but also because it provided the first clear example of surface faulting certainly related to coseismic displacement in the Apennines region and it shed light on some unknown and unexpected aspects of the earthquake generation process in the southern Apennines [*Westaway and Jackson*, 1984; *Pantosti and Valensise*, 1990; *Valensise and Pantosti*, 2001]. The interest raised by this event translated into a very abundant literature focused especially on the reconstruction of the rupture process based on joint analyses of different available observations and experimental data sets. For example, *Westaway and Jackson* [1984, 1987], who were the first to recognize field evidences for surface faulting, combined mainly field observations, teleseismic waveform modeling and earthquake relocation. *Bernard and Zollo* [1989] performed a detailed analysis of near-source strong motion records and leveling profiles, while *Pantosti and Valensise* [1990] tried to combine seismological and geodetic data with new field geologic investigations on the surface ruptures produced by the main shock. A very valuable data set is represented by 179 vertical deformation measurements collected by the Italian Military Geographic Institute (IGM) along the leveling points plotted as small black circles in Figure 8. The leveling lines had been surveyed in 1958–1959 and were resurveyed again just after the 1980 earthquake, so that the measured vertical changes can be reliably interpreted as coseismic deformations: details can be found in the work of *Arca and Marchioni* [1983] and *Arca et al.* [1983]. The geodetic data have been modeled through inversion procedures especially by *De Natale et al.* [1988] and *Pingue et al.* [1993], who analyzed the results in the light of the constraints put by other data.

[21] All of the cited papers agree on the conclusion that the November 23, 1980 earthquake was the result of a very complex process involving mainly normal faulting and that it involved the subsequent rupture of several fault segments with different geometries. According to the modeling performed by *Pingue et al.* [1993], the main shock rupture process involved three fault segments corresponding to three main subevents, occurring at 0 s, 18 s and 40 s after the nucleation. The subevents epicenters are plotted as black stars in Figure 8 and have been taken from *Bernard and Zollo* [1989]: the dashed segments represent the surface projections of the three faults upper edges, while the focal mechanisms reflect the source parameters listed by *Pingue et al.* [1993, Table 1], which the reader is referred to for further details.

[22] In our 2-D approach we cannot reproduce the complexity of the process, for which a complete 3-D model is needed. However, this is not crucial in the economy of the present study, and we can limit our analysis to the evaluation of the disturbances introduced by the local topography on the coseismic displacements produced by a single-fault

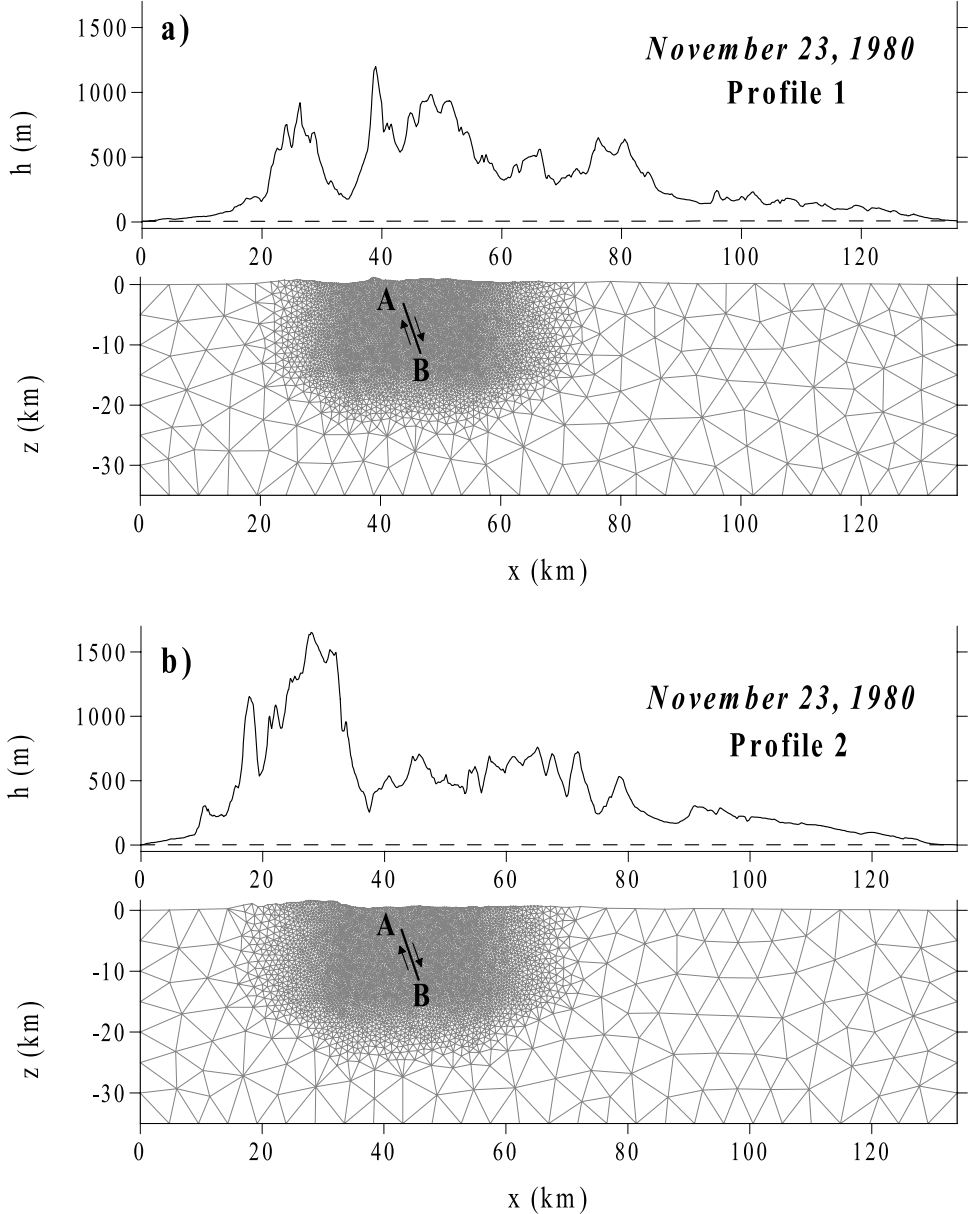


Figure 9. Surface topographic relief (with highly exaggerated vertical scale) and FE mesh for the cross-sections intersecting the Earth's surface along (a) profile 1 and (b) profile 2. Dashed lines are the FFS boundaries Δ_1 used to compute the ancillary Okada's solution on the crustal boundaries Γ_2 (see Figure 1b). The FE meshes are formed respectively by (a) 4994 nodes and 9788 elements and (b) 5210 nodes and 10,215 elements. Segment AB indicates the position and geometry of the NE dipping normal fault proposed by *De Natale et al.* [1988] and *Pingue et al.* [1993].

model such as that discussed by *De Natale et al.* [1988] and *Pingue et al.* [1993]. The surface projection of the single fault is represented by a black-bordered rectangle in Figure 8, while the relevant source parameters are listed in Table 2. We will perform our computations along two different vertical cross-sections, whose intersections with the Earth's free surface are indicated in Figure 8 by the two long solid segments numbered 1 and 2. Profile 1 intersects the fault surface projections in its central part, while profile 2 passes through the leveling point where the highest coseismic vertical deformation (≈ -74 cm) was measured. Figure 9 contains the topography shape along the two profiles and the

FE meshes built to discretize the two vertical cross sections. The position of the fault is indicated by the segments AB: in both cases, the fault lies under a relevant and highly variable free surface topography. We further observe that, in both cases, the two ends of the topographic profile have almost the same elevation, which reflects the case illustrated in Figure 1a. In other words, when computing the FFS analytic displacements, we will simply have to apply a translation along the z axis.

[23] The analysis we perform for the Irpinia earthquake is very similar to the one applied in section 3 for the Friuli event: we are interested in comparing the results obtained

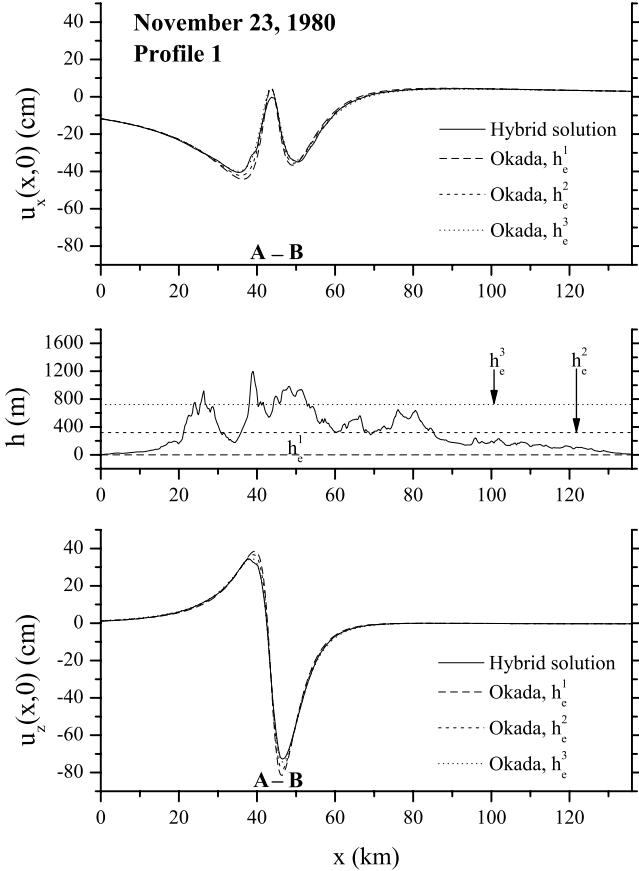


Figure 10. Horizontal (upper panel) and vertical (lower panel) surface coseismic displacements for the November 23, 1980 earthquake computed along profile 1. Segment AB indicates the surface projection of the fault shown in Figure 9a. The central panel contains the topographic relief and the three equivalent flat surface boundaries: $h_e^1 = 0$, $h_e^2 = 320$ m (topography averaged on the entire profile), $h_e^3 = 722$ m (topography averaged on the sub-interval $x \in [34, 56]$ km).

by means of our hybrid approach accounting for the irregular topography of the Earth's free surface to those computed through the Okada's solution. Figure 10 describes the results obtained along profile 1. Three flat reference levels h_e^1 , h_e^2 and h_e^3 have been chosen following the same criterion adopted in section 3: they are displayed in the central panel of Figure 10 together with the surface topography. The top and bottom panels illustrate the results concerning the horizontal and vertical displacements, respectively: we adopted the same vertical scale in the two plots. The first observation is that both the horizontal and the vertical signals are significantly altered by the topography: in the case of the vertical component the differences are limited approximately to the fault surface projection, while significant discrepancies among the horizontal signals are appreciable also some kilometers away from the fault upper edge projection. Concerning u_x , the hybrid solution is attenuated with respect to the FFS solutions obtained for h_e^1 and for h_e^2 in almost all the points along the profile: moreover, the negative peaks are found in

points placed more distant from the fault surface projection. When the comparison is made with the h_e^3 curve, we see that a better matching is obtained, especially in correspondence with the two negative peaks: on the opposite, the small positive maximum computed analytically near the projection of the fault shallower edge is not reproduced in the curve accounting for the topography effect.

[24] As regards the vertical deformation, it has already been noted that the relevant discrepancies between the result accounting for topography and those obtained for FFS are limited to points placed very close to the surface projection of the fault upper and lower edge (A and B respectively). Again, the solution computed through our approach is remarkably attenuated with respect to both the h_e^1 and h_e^2 analytical curves, while a satisfactory fit is found with the h_e^3 curve, i.e., with the analytical solution computed for a reference flat level coinciding with the average topography over a small distance containing the fault surface projection. The values for the misfits μ_x and μ_z and for the maximum absolute differences obtained along profile 1 are listed in Table 3: both misfits and absolute differences are computed between the hybrid solution and the analytical result valid for h_e^1 , and the computations have been limited to the small interval $x \in [39.5, 51]$ km. Note that the horizontal misfit is greater than the vertical one, while the opposite holds for

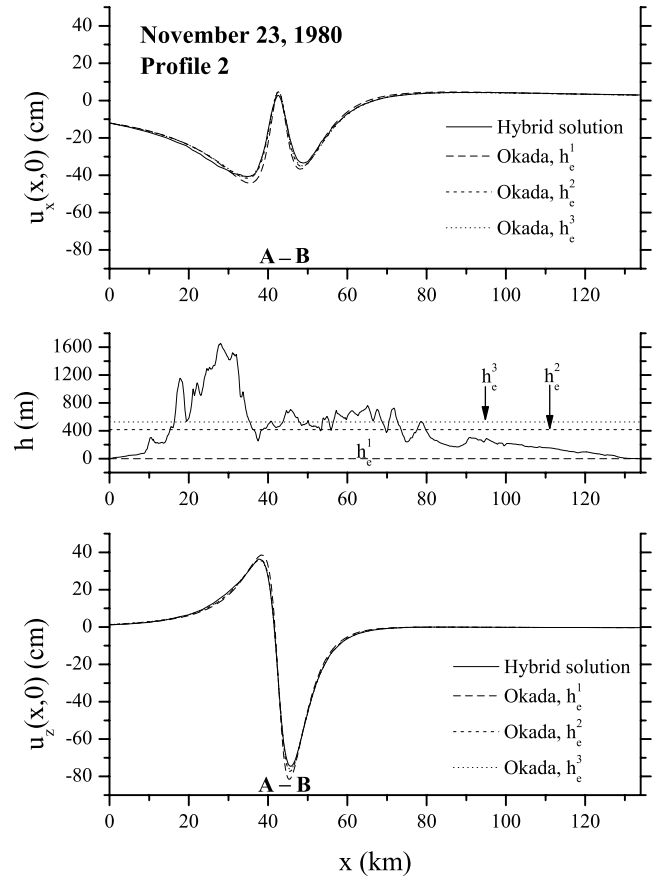


Figure 11. Same as Figure 10, but for profile 2. Segment AB is the surface projection of the fault shown in Figure 9b. The equivalent flat surface boundaries are: $h_e^1 = 0$, $h_e^2 = 416$ m (topography averaged on the entire profile), $h_e^3 = 527$ m (topography averaged on the sub-interval $x \in [33, 55]$ km).

the maximum absolute discrepancies. Note further that the value of 10.4 cm for $|\Delta u_z|_{\max}$ is by far greater than the typical errors associated with geodetic measures, and also about ten times the value obtained for the Friuli 1976 earthquake.

[25] The results obtained along profile 2 are described in Figure 11. Some interesting differences can be observed in the comparison between the topographic shapes along the two profiles (see central panels of Figures 10 and 11). First, the relief in correspondence with the fault surface projection along profile 2 is smaller than along profile 1, which implies that the fault upper edge is closer to the free surface along the second profile. As a consequence, the positive and negative peaks in the vertical hybrid signal are slightly greater than those computed for profile 1; concerning the horizontal displacement, the small local positive maximum characterizing the FFS analytical solutions in correspondence with the fault upper edge is now reproduced also by the hybrid solution. Moreover, in the case of profile 2, the flat reference level h_e^3 , coinciding with the topography averaged in the domain $x \in [33, 55]$ km, is very similar to h_e^2 (topography averaged along the entire profile). This implies that the FFS solutions relative to h_e^2 and h_e^3 are very similar, and it can be observed from the upper and lower panels in Figure 11 that they are the analytical solutions that best approximate the hybrid results; instead, relevant discrepancies are found between the solution accounting for topography and the h_e^1 analytical curve. Finally, approximately in the interval $x \in [15, 35]$ km, profile 2 cuts across a massif with maximum heights above 1600 m: in the same distance interval, profile 1 is characterized by less pronounced and less extended topographic structures. This is reflected especially in the horizontal displacement component (upper panel in Figure 11): it can be appreciated that a small but non-negligible difference exists between the hybrid and the Okada's curves even at 20 km from the fault upper edge projection.

[26] The values for μ_x , μ_z , $|\Delta u_x|_{\max}$ and $|\Delta u_z|_{\max}$ computed along profile 2 are listed in the last row of Table 3. Apart from μ_x , all the other quantities are slightly smaller for profile 2 than for profile 1. Anyhow, the maximum absolute differences are still significant and markedly greater than the typical geodetic errors.

[27] The quantitative results concerning the misfits and the availability of leveling data for the November 23, 1980 Irpinia earthquake tempted us to undertake the comparison of our model predictions with the experimental data. We are perfectly conscious of the intrinsic limitations of our 2-D approach: neglecting the finiteness of the fault and the topography variation in the third dimension are indeed severe limits that don't allow us to model the entire set of geodetic observations. Anyhow, we can overcome such difficulties, at least partially, if we select a profile placed not too close to the fault terminations (in the strike direction) and if we restrict our attention to a small subset of the experimental data, namely only to points placed at distances from the profile lower than a given value (for example 1 km). We present the results obtained in the case of profile 2, which we selected because it passes through the geodetic benchmark where the highest vertical deformation (≈ -74 cm) was measured. Figure 12 shows the experimental vertical deformations collected in seven leveling bench-

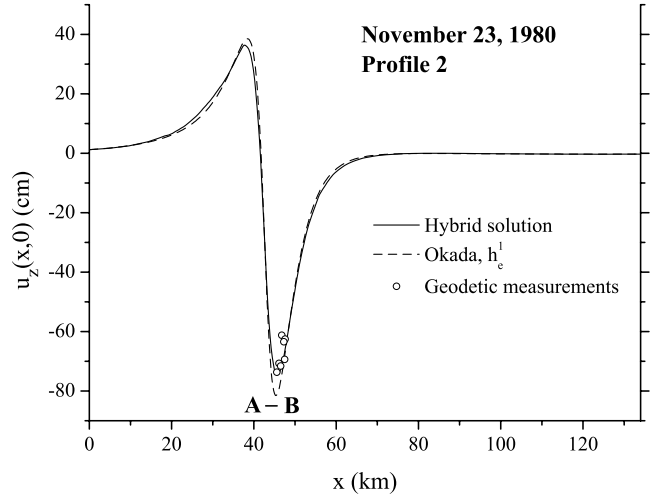


Figure 12. Open circles are the experimental leveling measures collected in seven benchmarks placed “close” to profile 2 (i.e., at distances lower than 1 km). The solid and dashed lines are the theoretical curves computed through our hybrid method, accounting for the topographic effect, and through Okada's FFS model for $h_e^1 = 0$, respectively.

marks placed close to profile 2, and the vertical displacements computed through our hybrid model and through Okada's formulae for h_e^1 . The solution accounting for topography is able to fit very satisfactorily the maximum experimental vertical displacements, while Okada's curve shows a marked overestimation.

5. Conclusions

[28] The problem faced in the present study regarded the theoretical computation of the disturbances introduced by the irregular topography of the Earth's free surface on the coseismic displacement field produced by a crustal earthquake. We adopted the model recently introduced by T&A, which is valid for 2-D purely elastic and homogeneous domains bounded by a free surface that can assume any irregular shape. The original model by T&A required the two ends of the topographic profile to have equal or very similar elevations: here it has been generalized to deal with the more general case in which the two ends have different elevations. The method can be defined a two-step hybrid approach, since the final solution for the coseismic displacement field is determined as the sum of two distinct terms, that are computed in two different steps and with different techniques. The first term (ST) is related to the seismic source mechanism: it is computed through the analytical formulae valid for faults embedded in a homogeneous, elastic unbounded space [e.g., Okada, 1992]. The second term (FSC) is the correction that must be added to the ST displacements when a free surface is introduced. The FSC can be computed in closed analytical form only when the free surface is flat (Okada [1985, 1992]): in all the other cases, approximate analytical and/or numerical techniques must be adopted. The technique adopted here (T&A) computes FSC through a finite element code, developed by the authors, which solves the equations of elastic equilibrium in two dimensions in the plane-strain approximation.

[29] Concerning the theoretical aspects of the problem, we devoted some attention to the comparison between our hybrid method and the models based exclusively on the FE technique. The most relevant difference consists in the way the fault and the coseismic displacements in correspondence of it are represented in the two approaches. Pure FE codes must include explicitly the fault on the computational mesh and prescribe the displacements (absolute or relative) on its nodes as known boundary conditions. While it is possible to determine the ST displacements analytically whatever the free surface shape is, it is not possible to compute the FSC “*a priori*” when the free surface is not flat. In these cases, pure FE models cannot completely account for FSC. On the other hand, the adoption of a two-step approach like ours guarantees that both ST and FSC are correctly accounted for, even in presence of an irregular topography. Moreover, we are not obliged to introduce the fault into the FE mesh, which brings the interesting practical advantage that the same mesh can be used for faults with similar positions but different geometric and focal parameters. After showing the very good agreement between the solution obtained by means of our technique and the Okada’s one in the reference case of a FFS, we compared the hybrid and the pure FE approaches on the same reference case: in the pure FE case, we made two different choices for the displacements to be assigned on the fault boundary, namely the complete ST displacement field and the sole tangential ST component. For both choices, we found significant discrepancies with respect to the solution obtained through our method. The discrepancies are evident mainly on the horizontal component when the tangential ST is imposed (with misfits as large as 35%), while they characterize both horizontal and vertical components when the complete ST field is prescribed on the fault (with misfits than can exceed 20% for both cases).

[30] We applied our 2-D technique to two real earthquakes occurred in Italy in the last thirty years, namely the May 6, 1976 event occurred in Friuli and the November 23, 1980 shock with epicenter in the Irpinia-Basilicata region. The choice was suggested by the fact that both earthquakes occurred in regions with relevant topographic features: the first in correspondence with the south-eastern Alpine relief, the second on the southern portion of the Apennines chain. Some objections could be made regarding the choice of these two particular events, since it is widely accepted in the literature that they both involved complex multiple fault geometries, so that only a fully 3-D model could allow for a complete description of the earthquakes’ features. Anyhow, the goal of this study was not the critical discussion of the available source models, nor the introduction of alternative hypotheses, nor the inversion of any particular data set. Rather, we were interested in the estimation of the topography disturbances on the surface displacements via a forward approach and in the comparison between the results predicted by our model and those obtained through the Okada’s solution valid for FFS, which is still widely employed in both direct and inverse modeling of geodetic data, even in regions with highly irregular topography. From this point of view, a 2-D approach should be regarded as fully acceptable and sufficient to draw some basic conclusions; further, we can adopt simpler single-fault models available in the literature as test cases without any particular

loss in generality. Since we work in the 2-D plane-strain approximation, in each of the treated examples the fault length is assumed as theoretically infinite. We applied the same approximation also in the Okada’s analytical model by assuming $L = 20W$, L and W being the fault’s length and width, respectively. Moreover, in all the proposed examples the analytical signals have been computed by introducing three distinct flat reference elevations h_e , corresponding to the “zero elevation” and to the average topography computed along the entire profile or on the points belonging to a narrow interval around the fault surface projection. The following points summarize the main results of our analysis.

[31] 1. The perturbations introduced by the local topography are mainly related to amplification/reduction of the surface displacements with respect to those computed for FFS: the greatest differences are observed in correspondence and in proximity of the fault’s surface projection, while at long wavelengths no significant difference is observed between the two solutions.

[32] 2. The component on which topography induces the more evident perturbations, at least in the sense of percentage misfit, is the horizontal. This can be appreciated, for example, by looking at Table 3. Note that, in the case of the 1976 Friuli earthquake, none of the analytical solutions is able to provide a good fit to our solution.

[33] 3. The horizontal displacements experience also minor high-frequency-content alterations on the points belonging to the fault surface projection. A finer resolution of the FE mesh may possibly allow for a clearer detection of such alterations.

[34] 4. Concerning the vertical component, the discrepancies are limited to very narrow intervals around the surface projections of the fault upper and lower edges. For the 1976 case, only minor effects are introduced by the topography, and the best fit is given by the analytical signal computed for the “zero reference level”. In other words, the solution including the topographic effect and the usual Okada’s solution are the same, in the sense that their difference is of the same order of the typical errors of the geodetic measures. The results for the 1980 Irpinia earthquake are completely different. Depending on the particular profile studied, the average misfit can be as high as 13% and, locally, differences up to 10 cm can be observed (See Table 3). In this case, the observed discrepancies are markedly bigger than the typical geodetic errors. Moreover, the modeling performed along profile 2 (see Figure 12) demonstrates that we can fit very satisfactorily the experimental geodetic data collected on benchmarks lying very close to the profile itself.

[35] 5. In general, an important role is played by the position of the fault relative to the main topographic features. The source selected for the 1976 Friuli earthquake is placed near the boundary of the south-eastern Alpine chain and the perturbation introduced by the topography on the coseismic displacements are much smaller than those computed for the case of the 1980 event, whose parent fault is placed entirely under the southern Apennines relief.

[36] It is worth observing that the general conclusions drawn in points 1–5 confirm the results obtained by T&A in their study applied to the 1997 Umbria-Marche (Italy) earthquake sequence.

[37] The methodology adopted in this paper is based on very simple hypotheses both for the 2-D medium (homogeneous and isotropic) and for the fault geometry (single rectangular faults with homogeneous slip distribution). Since the same approximations are also adopted in the basic Okada's model, we can conclude that the discrepancies we found in all the studied examples are to be imputed solely to the topography effect. Indeed, more realistic approaches should account for the heterogeneities of the crust structure, for the non-planar shape of the fault and for slip gradients on the fault itself, and there is no doubt that these factors are expected to play non-negligible effects on the final coseismic deformation pattern. Anyhow, unlike all the previous characteristics, topography can be known with great detail and the modeling of its effect should be the primary step in any forward, and even inverse, approach.

[38] As a final remark, the study performed in this paper is far from being a thorough treatment of the problem of the topography effect on coseismic displacements. A fully 3-D model will be required to gain a more exhaustive understanding of the local and, perhaps, the regional disturbances induced by the irregular topography of the Earth's free surface. The development of a 3-D model is the main objective of our future research: in our hybrid scheme, the major goal is that of developing a numerical code based on FE or BE (Boundary Elements) for the computation of FSC on 3-D domains.

[39] **Acknowledgments.** The authors are grateful to the DIIAR-Politecnico di Milano (Italy) for providing the Italian DTM, and particularly to Professor Riccardo Barzaghi and his collaborators. This work was financed by the Italian "Ministero dell'Istruzione, dell'Università e della Ricerca" (MIUR, formerly named "Ministero dell'Università e della Ricerca Scientifica e Tecnologica" (MURST)).

References

- Anderson, H., and J. Jackson, Active tectonics in the Adriatic region, *Geophys. J. R. Astron. Soc.*, **91**, 937–983, 1987.
- Arca, S., and A. Marchioni, I movimenti verticali del suolo nelle zone della Campania e della Basilicata interessate dal sisma del novembre 1980 (in Italian), *Boll. Geod. Sci. Aff.*, **42**(2), 126–135, 1983.
- Arca, S., V. Bonasia, R. Gaulon, F. Pingue, J. C. Ruegg, and R. Scarpa, Ground movements and faulting mechanism associated with the November 23, 1980 Southern Italy earthquake, *Boll. Geod. Sci. Aff.*, **42**(2), 137–147, 1983.
- Armigliato, A., S. Tinti, and A. Manucci, Self-induced deformation on the fault plane during an earthquake. Part I: Continuous normal displacements, *Pure Appl. Geophys.*, **160**, 1651–1678, 2003a.
- Armigliato, A., S. Tinti, and A. Manucci, Self-induced deformation on the fault plane during an earthquake. Part II: Continuous tangential displacements, *Pure Appl. Geophys.*, **160**, 1679–1693, 2003b.
- Aoudia, A., A. Saraò, B. Bukchin, and P. Suhadolc, The 1976 Friuli (NE Italy) thrust faulting earthquake: A reappraisal 23 years later, *Geophys. Res. Lett.*, **27**, 573–576, 2000.
- Bernard, P., and A. Zollo, The Irpinia (Italy) 1980 earthquake: Detailed analysis of a complex normal fault, *J. Geophys. Res.*, **94**, 1631–1648, 1989.
- Bonafede, M., and A. Neri, Effects induced by an earthquake on its fault plane: A boundary element study, *Geophys. J. Int.*, **141**, 43–56, 2000.
- Boschi, E., E. Guidoboni, G. Ferrari, G. Valensise, and P. Gasperini, Catalogo dei forti terremoti in Italia dal 461 a. C. al 1990, 644 pp., Ist. Nazion. di Geofis. and Storia Geofis. Ambiente, Bologna, Italy, 1997.
- Bressan, G., A. Snidarcig, and C. Venturini, Present state of tectonic stress of the Friuli area (eastern Southern Alps), *Tectonophysics*, **292**, 211–227, 1998.
- Briole, P., G. De Natale, R. Gaulon, F. Pingue, and R. Scarpa, Inversion of geodetic data and seismicity associated with the Friuli earthquake sequence (1976–1977), *Ann. Geophys. B*, **4**, 481–492, 1986.
- De Natale, G., F. Pingue, and R. Scarpa, Seismic and ground deformation monitoring in the seismogenic region of the southern Apennines, Italy, *Tectonophysics*, **152**, 165–178, 1988.
- Harrison, J. C., Cavity and topographic effects in tilt and strain measurements, *J. Geophys. Res.*, **81**, 319–328, 1976.
- Huang, B., and Y. T. Yeh, Effect of near-fault terrain upon dislocation modeling, *Pure Appl. Geophys.*, **150**, 1–18, 1997.
- McTigue, D. F., and C. C. Mei, Gravity-induced stresses near topography of small slope, *J. Geophys. Res.*, **86**, 9268–9278, 1981.
- McTigue, D. F., and P. Segall, Displacements and tilts from dip-slip faults and magma chambers beneath irregular surface topography, *Geophys. Res. Lett.*, **15**, 601–604, 1988.
- McTigue, D. F., and R. Stein, Topographic amplification of tectonic displacement: Implications for geodetic measurement of strain changes, *J. Geophys. Res.*, **89**, 1123–1131, 1984.
- Meertens, C. M., and J. M. Wahr, Topographic effect on tilt, strain, and displacement measurements, *J. Geophys. Res.*, **91**, 14,057–14,062, 1986.
- Melosh, H. J., and A. Raefsky, A simple and efficient method for introducing faults into finite element computations, *Bull. Seism. Soc. Am.*, **71**, 1391–1400, 1981.
- Okada, Y., Surface deformation due to shear and tensile faults in a half-space, *Bull. Seism. Soc. Am.*, **75**, 1135–1154, 1985.
- Okada, Y., Internal deformation due to shear and tensile faults in a half-space, *Bull. Seism. Soc. Am.*, **82**, 1018–1040, 1992.
- Pantosti, D., and G. Valensise, Faulting mechanism and complexity of the November 23, 1980, Campania-Lucania earthquake, inferred from surface observations, *J. Geophys. Res.*, **95**, 15,319–15,341, 1990.
- Pingue, F., G. De Natale, and P. Briole, Modeling of the 1980 Irpinia earthquake source: Constraints from geodetic data, *Ann. Geofis.*, **36**, 27–40, 1993.
- Pondrelli, S., G. Ekström, and A. Morelli, Seismotectonic re-evaluation of the 1976 Friuli, Italy, seismic sequence, *J. Seismol.*, **5**, 73–83, 2001.
- Slejko, D., G. Neri, I. Orozova, G. Renner, and M. Wyss, Stress field in Friuli (NE Italy) from fault plane solutions of activity following the 1976 main shock, *Bull. Seismol. Soc. Am.*, **89**, 1037–1052, 1999.
- Talamo, R., M. Pampaloni, and S. Grassi, Risultati delle misure di livellazione di alta precisione eseguite dall'Istituto Geografico Militare nelle zone del Friuli interessate dalle recenti attività sismiche (in Italian), *Boll. Geod. Sci. Aff.*, **37**, 61–75, 1978.
- Tinti, S., and A. Armigliato, A 2-D hybrid technique to model the effect of topography on coseismic displacements: Application to the Umbria-Marche (central Italy) 1997 earthquake sequence, *Geophys. J. Int.*, **150**, 542–557, 2002.
- Valensise, G., and D. Pantosti, The investigation of potential earthquake sources in peninsular Italy: A review, *J. Seismol.*, **5**, 287–306, 2001.
- Voevoda, O. D., and L. N. Volynets, The topography of the ground surface and postseismic displacements, *Comput. Seismol. Geodyn.*, **2**, 58–63, 1992.
- Volynets, L. N., and O. D. Voevoda, Deformations of a free boundary caused by an internal fault, *Comput. Seismol. Geodyn.*, **2**, 50–57, 1992.
- Westaway, R., and J. Jackson, Surface faulting in the southern Italian Campania-Basilicata earthquake of 23 November 1980, *Nature*, **312**, 436–438, 1984.
- Westaway, R., and J. Jackson, The earthquake of 1980 November 23 in Campania-Basilicata (southern Italy), *Geophys. J. R. Astron. Soc.*, **90**, 375–443, 1987.
- Williams, C. A., and J. Wadge, An accurate and efficient method for including the effects of topography in three-dimensional elastic models of ground deformation with applications to radar interferometry, *J. Geophys. Res.*, **105**, 8103–8120, 2000.
- Zollo, A., A. Bobbio, A. Emolo, and A. Herrero, Modelling of ground acceleration in the near source range: The case of 1976, Friuli earthquake ($M = 6.5$), northern Italy, *J. Seismol.*, **1**, 305–319, 1997.

A. Armigliato and S. Tinti, Department of Physics, Sector of Geophysics, University of Bologna, Bologna I-40127, Italy. (armigliato@ibogfs.dfm.unibo.it; steve@ibogfs.dfm.unibo.it)